Benchmarking Substellar Evolutionary Models Using New Age Estimates for HD 4747 B and HD 19467 B

Charlotte M. Wood[1] , Tabetha Boyajian[2] , Kaspar von Braun[3] , John M. Brewer[4,5] , Justin R. Crepp[1] , Gail Schaefer[6] ,
Arthur Adams[4] , and Timothy R. White[7]

[1] University of Notre Dame, Department of Physics, 225 Nieuwland Science Hall, Notre Dame, IN 46556, USA; cwood12@nd.edu
[2] Louisiana State University, Department of Physics and Astronomy, 202 Nicholson Hall, Baton Rouge, LA 70803, USA
[3] Lowell Observatory, 1400 W Mars Hill Road, Flagstaff, AZ 86001, USA
[4] Yale University, Department of Astronomy, P.O. Box 208101, New Haven, CT 06520, USA
[5] Columbia University, Department of Astronomy, Mail Code 5246, 550 West 120th Street, New York, NY 10027, USA
[6] The CHARA Array of Georgia State University, Mount Wilson, CA 91023, USA
[7] Stellar Astrophysics Centre, Department of Physics and Astronomy, Aarhus University, Ny Munkegade 120, DK-8000 Aarhus C, Denmark

Abstract

Constraining substellar evolutionary models (SSEMs) is particularly difficult due to a degeneracy between the mass, age, and luminosity of a brown dwarf. In cases where a brown dwarf is found as a directly imaged companion to a star, as in HD 4747 and HD 19467, the mass, age, and luminosity of the brown dwarf are determined independently, making them ideal objects to use to benchmark SSEMs. Using the Center for High Angular Resolution Astronomy Array, we measured the angular diameters and calculated the radii of the host stars HD 4747 A and HD 19467 A. After fitting their parameters to the Dartmouth Stellar Evolution Database, MESA Isochrones and Stellar Tracks, and Yonsei-Yale isochronal models, we adopt age estimates of $10.74^{+6.75}_{-6.87}$ Gyr for HD 4747 A and $10.06^{+1.16}_{-0.82}$ Gyr for HD 19467 A. Assuming the brown dwarf companions HD 4747 B and HD 19467 B have the same ages as their host stars, we show that many of the SSEMs under-predict bolometric luminosities by $\sim$0.75 dex for HD 4747 B and $\sim$0.5 dex for HD 19467 B. The discrepancies in luminosity correspond to over-predictions of the masses by $\sim$12% for HD 4747 B and $\sim$30% for HD 19467 B. We also show that SSEMs that take into account the effect of clouds reduce the under-prediction of luminosity to $\sim$0.6 dex and the over-prediction of mass to $\sim$8% for HD 4747 B, an L/T transition object that is cool enough to begin forming clouds. One possible explanation for the remaining discrepancies is missing physics in the models, such as the inclusion of metallicity effects.

Key words: brown dwarfs – stars: evolution – stars: individual (HD4747, HD19467) – techniques: high angular resolution – techniques: interferometric

Supporting material: figure set

1. Introduction

The atmospheres of brown dwarfs are quite complicated, including multiple convection zones, the possibility of cloud formation, and the presence of molecules that results in highly wavelength-dependent opacities (Marley & Robinson 2015). Atmospheric effects are also the main factor in determining how a brown dwarf evolves and cools. If we hope to fully understand brown dwarfs and other substellar objects, we need models that take into account all of these effects. Having complete models is especially important when studying free-floating "field" brown dwarfs, whose properties cannot be determined other than from the atmosphere.

Recent substellar evolutionary models (SSEMs) do a better job of predicting optical color of brown dwarfs and matching observations for older objects than their predecessors (Baraffe et al. 2015). However, tests of these models are still fairly limited due to degeneracies between mass, age, and luminosity for brown dwarfs; a young, less massive brown dwarf can appear to have the same luminosity as an old, more massive brown dwarf. These degeneracies are the main sources of uncertainty in age estimates for field brown dwarfs, inhibiting the accuracy of model tests. To properly constrain the models, we need benchmark brown dwarfs—objects whose masses, ages, and luminosities can be determined independently.

The mass of a benchmark brown dwarf can be calculated using the orbital mechanics of the system in which it is found (Liu et al. 2008; Dupuy et al. 2009a; Crepp & Johnson 2011; Dupuy & Liu 2017). Other properties of a benchmark brown dwarf—such as age and metallicity—can be more readily inferred by studying the host star rather than the brown dwarf itself.

Using isochronal models, a more accurate age estimate of the host star can be determined by measuring the precise stellar radius, which places additional constraints on the location of the star on the HR-diagram (Crepp et al. 2012). For nearby stars ($d \leqslant 50$ parsec), it is possible to determine the stellar radius precisely using interferometry (Boyajian et al. 2012a, 2012b).

In this paper, we present angular diameter measurements from the Center for High Angular Resolution Astronomy (CHARA) Array and calculate the radius (Section 2) of two Sun-like stars, HD 4747 A and HD 19467 A, known to host benchmark brown dwarf companions (Crepp et al. 2014, 2016, 2018). We also present new age estimates for these systems (Section 4) using the Dartmouth Stellar Evolution Database, MESA Isochrones and Stellar Tracks (MIST), and Yonsei-Yale (YY) isochrone models (Dotter et al. 2007, 2008; Paxton et al. 2011, 2013, 2015; Spada et al. 2013; Choi et al. 2016; Dotter 2016). Assuming that the directly imaged brown
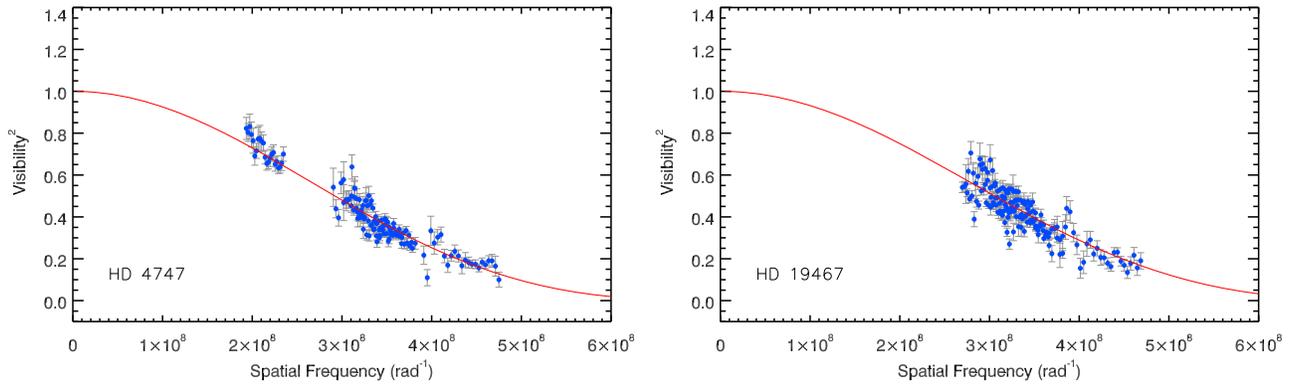
Figure 1. Calibrated interferometric V^2 values (points) and the R-band, limb-darkened fits to those measurements (line) for HD 4747 (left) and HD 19467 (right). The units of the x-axis correspond to the baseline length in units of operational wavelength. For more details, see Section 2.

Table 1
Observation Log

Object	UT Date	CHARA Baseline	Calibrator
HD 4747	2015 Aug 14	W1-E1 (313.53 m)	HD 4622
	2016 Aug 1	W2-E2 (156.27 m)	HD 4622
	2016 Nov 11	W1-E2 (251.34 m)	HD 2696, HD 4622
HD 19467	2014 Sep 6	E1-S1 (330.66 m)	HD 17943, HD 22243
	2014 Sep 7	W1-E1 (313.53 m)	HD 17943, HD 22243
	2015 Aug 17	E2-S1 (278.76 m)	HD 17943, HD 22243
	2016 Nov 11	W1-E2 (251.34 m)	HD 16141, HD 17943, HD 22243

Note. Refer to Section 2 for details.

dwarf companions HD 4747 B and HD 19467 B have the same ages as their respective host stars, we use the isochronal age estimates to test and constrain several SSEMs (Section 6; Chabrier et al. 2000; Baraffe et al. 2002, 2003, 2015; Saumon & Marley 2008). Both benchmark brown dwarfs have precisely measured dynamical masses and metallicities, making them ideal objects to calibrate models.

## 2. Interferometric Observations and Stellar Radii

In order to obtain direct estimates for the stellar diameters, we performed interferometric observations with Georgia State University's CHARA Array, a long-baseline optical/infrared interferometer located within the Mount Wilson Observatory in California. The CHARA Array consists of six 1 m diameter telescopes with distances between telescopes ranging from ~30–330 m (ten Brummelaar et al. 2005). The predicted angular sizes of HD 4747 A and HD 19467 A, based on the surface brightness relations in Boyajian et al. (2014), are on the order of a few tenths of a milliarcsecond (mas). Thus, we conducted our observations using the PAVO beam combiner (Ireland et al. 2008) in the R-band with the baseline configurations listed in Table 1 in order to adequately resolve the stars.

HD 4747 A was observed during the nights of 2015 August 14 UT, 2016 August 1 UT, and 2016 November 11 UT. HD 19467 A was observed during the nights of 2014 September 6 and 7 UT, 2015 August 17 UT, and 2016 November 11 UT. The observations of our targets are bracketed in time with several calibrator stars, the selection of which is based on the JMMC Stellar Diameters Catalog (JSDC; Duvert 2016).[8] In order to identify and thus avoid unknown systematic errors in our

interferometry data, we require the use of at least two calibrator stars per target, the use of at least two combinations of telescopes (baselines), and data from at least two nights. Calibrator stars for HD 4747 A are HD 2696 ($\theta_{UD,R} = 0.34 \pm 0.03$ mas) and HD 4622 ($\theta_{UD,R} = 0.219 \pm 0.006$ mas). Calibrators for HD 19467 A are HD 16141 ($\theta_{UD,R} = 0.366 \pm 0.010$ mas), HD 17943 ($\theta_{UD,R} = 0.234 \pm 0.007$ mas), and HD 22243 ($\theta_{UD,R} = 0.185 \pm 0.005$ mas) (Chelli et al. 2016; Duvert 2016). These calibrators are selected based upon their physical attributes: no known multiplicity, low projected rotational velocity, similar brightness as the respective target in R, close angular proximity (max 10°) to the respective science target, and to be unresolved sources based on their estimated angular sizes (van Belle & van Belle 2005; Boyajian et al. 2013; von Braun et al. 2014). A summary of our observations is shown in Table 1.

Our data reduction procedure to extract calibrated squared-visibility measurements (V^2, Figure 1) is described in Section 2.1 in Boyajian et al. (2015) and is based on the methods outlined in Maestro et al. (2013) and White et al. (2013). We measure uniform disk angular diameters of $\theta_{UD} = 0.367 \pm 0.006$ mas for HD 4747 A and $\theta_{UD} = 0.355 \pm 0.011$ mas for HD 19467 A. We determine limb-darkened angular diameters of $\theta_{LD} = 0.390 \pm 0.007$ mas for HD 4747 A and $\theta_{LD} = 0.376 \pm 0.014$ mas for HD 19467 A using respective limb-darkening coefficients of $\mu_R = 0.63$ and $\mu_R = 0.60$ (Claret & Bloemen 2011). Combined with parallaxes from *Gaia* DR2 (Gaia Collaboration et al. 2018), we obtain stellar radii of $R = 0.789 \pm 0.014\,R_\odot$ for HD 4747 A and $R = 1.295 \pm 0.048\,R_\odot$ for HD 19467 A (Table 2). Our new radius measurements are consistent with literature values within 1σ for HD 4747 A (Crepp et al. 2018) and within 3σ for HD 19467 A (Crepp et al. 2014).

---

[8] http://www.jmmc.fr/jsdc
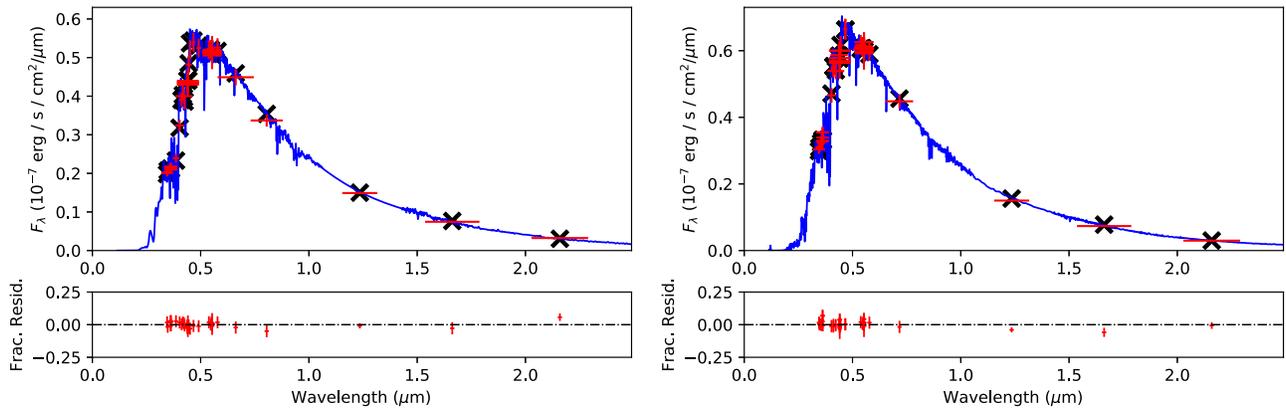
Figure 2. SED fits for HD 4747 A (left) and HD 19467 A (right). Pickles (1998) spectral templates (blue lines; G8V for HD 4747 A, G2V for HD 19467 A) are scaled to the literature photometry (red crosses). Black crosses show the flux value of the spectral template integrated over the filter transmission profile. The lower panels display residuals between literature photometry and the spectral template. See Section 3 for more details.

Table 2
Properties of the Host Stars

Property	HD 4747 A	HD 19467 A
R.A. (J2000)	00 49 26.77	03 07 18.57
Decl. (J2000)	−23 12 44.93	−13 45 42.42
Spectral Type	G9V[a]	G3V[b]
Parallax (mas)[c]	53.184 ± 0.126	31.225 ± 0.041
Distance (pc)	18.80 ± 0.04	32.02 ± 0.04
Mass ($M_\odot$)	0.82 ± 0.04[a]	0.95 ± 0.02[b]
[Fe/H]	−0.22 ± 0.04[a]	−0.15 ± 0.02[b]
$\log(g)$ (cm s^{-2})	4.65 ± 0.06[a]	4.40 ± 0.06[b]
$\theta_{\rm UD}$ (mas)[d]	0.367 ± 0.006	0.355 ± 0.011
$\theta_{\rm LD}$ (mas)[d]	0.390 ± 0.007	0.376 ± 0.014
Radius ($R_\odot$)[d]	0.789 ± 0.014	1.295 ± 0.048
$F_{\rm BOL}$ (10^{-8} erg s^{-1} cm^{-2})[d]	4.02 ± 0.03	4.54 ± 0.03
Luminosity ($L_\odot$)[d]	0.444 ± 0.004	1.456 ± 0.010
$T_{\rm eff,interferometric}$ (K)[d]	5308 ± 48	5572 ± 104
$T_{\rm eff,spectroscopic}$ (K)[d,e]	5305 ± 25	5748 ± 25

Notes.
[a] Crepp et al. (2016).
[b] Crepp et al. (2014).
[c] Gaia Collaboration et al. (2018).
[d] This paper (Sections 2–4).
[e] Statistical uncertainty only, does not include model uncertainty.

3. Bolometric Fluxes, Stellar Effective Temperatures, and Stellar Luminosities

Coupled with stellar angular diameter, the knowledge of stellar bolometric flux ($F_{\rm BOL}$) provides a direct estimate of stellar temperature, which, when combined with physical stellar radius, yields stellar luminosity via a reformulation of the Stefan–Boltzmann Law,

$$T_{\rm eff}({\rm K}) = 2341(F_{\rm BOL}/\theta_{\rm LD}^2)^{\frac{1}{4}}, \qquad (1)$$

where $F_{\rm BOL}$ has units of 10^{-8} erg cm^{-2} s^{-1} and $\theta_{\rm LD}$ has units of milliarcseconds. $F_{\rm BOL}$ can be obtained by spectral energy distribution (SED) fitting by scaling spectral templates to literature photometry values. For the SED fitting of our targets (Figure 2), we follow the approach used in Mann et al. (2013) and von Braun et al. (2014). Interstellar extinction is set to zero

for both targets due to the small distances to our targets (less than 70 pc)[9] and we use the updated broadband filter profiles presented in Mann & von Braun (2015). In the calculation of the errors in effective temperature and stellar luminosity, we inflate the calculated uncertainty in our $F_{\rm BOL}$ (as given below) by adding 2% of the error in quadrature, thereby compensating for unknown systematic errors in the literature photometry (Bohlin et al. 2014).

Based on fitting a G8V spectral template from the Pickles (1998)[10] library to literature photometry from Irwin (1961), Stoy (1963), Wild (1969), Mermilliod (1986), Rufener (1988), Mermilliod & Nitschelm (1989), Olsen (1993), Hauck & Mermilliod (1998), Cutri et al. (2003), and Koen et al. (2010), we measure HD 4747 A's $F_{\rm BOL}$ to be $(4.02 ± 0.03) \times 10^{-8}$ erg s^{-1} cm^{-2}, which, when combined with angular diameter as stated in Equation (1), produces $T_{\rm eff} = 5308 ± 48$ K and a luminosity of $L = 0.444 ± 0.004\,L_\odot$. Compared to previous literature values, our new temperature estimate for HD 4747 A is consistent within 1σ (Crepp et al. 2018).

Using the same approach, we fit a G2V spectral template from the Pickles (1998) library to literature photometry from Corben (1971), Corben et al. (1972), Olsen (1983), Eggen (1983), Mermilliod (1986), Rufener (1988), Olsen (1994), Kornilov et al. (1996), Hauck & Mermilliod (1998), and Cutri et al. (2003) to obtain HD 19467 A's $F_{\rm BOL}$ to be $(4.54 ± 0.03) \times 10^{-8}$ erg s^{-1} cm^{-2}. Based on the stellar angular diameter, this yields $T_{\rm eff} = 5573 ± 104$ K (Equation (1)) and a luminosity of $L = 1.456 ± 0.010\,L_\odot$. Compared with previous literature values, our new temperature estimate for HD 19467 A is consistent within 2σ (Crepp et al. 2014).

4. Stellar Age Estimates

We derived age estimates for HD 4747 A and HD 19467 A using three different sets of isochrones and two different interpolation procedures. For each estimate, we started with stellar parameters derived from high resolution ($R \sim 70,000$) spectra of the two stars from the Keck HIRES spectrograph (Vogt et al. 1994), analyzed using the procedure in Brewer et al. (2016).

[9] See Aumer & Binney (2009) for more details.
[10] See also https://lco.global/~apickles/INGS/ for updated spectral templates.
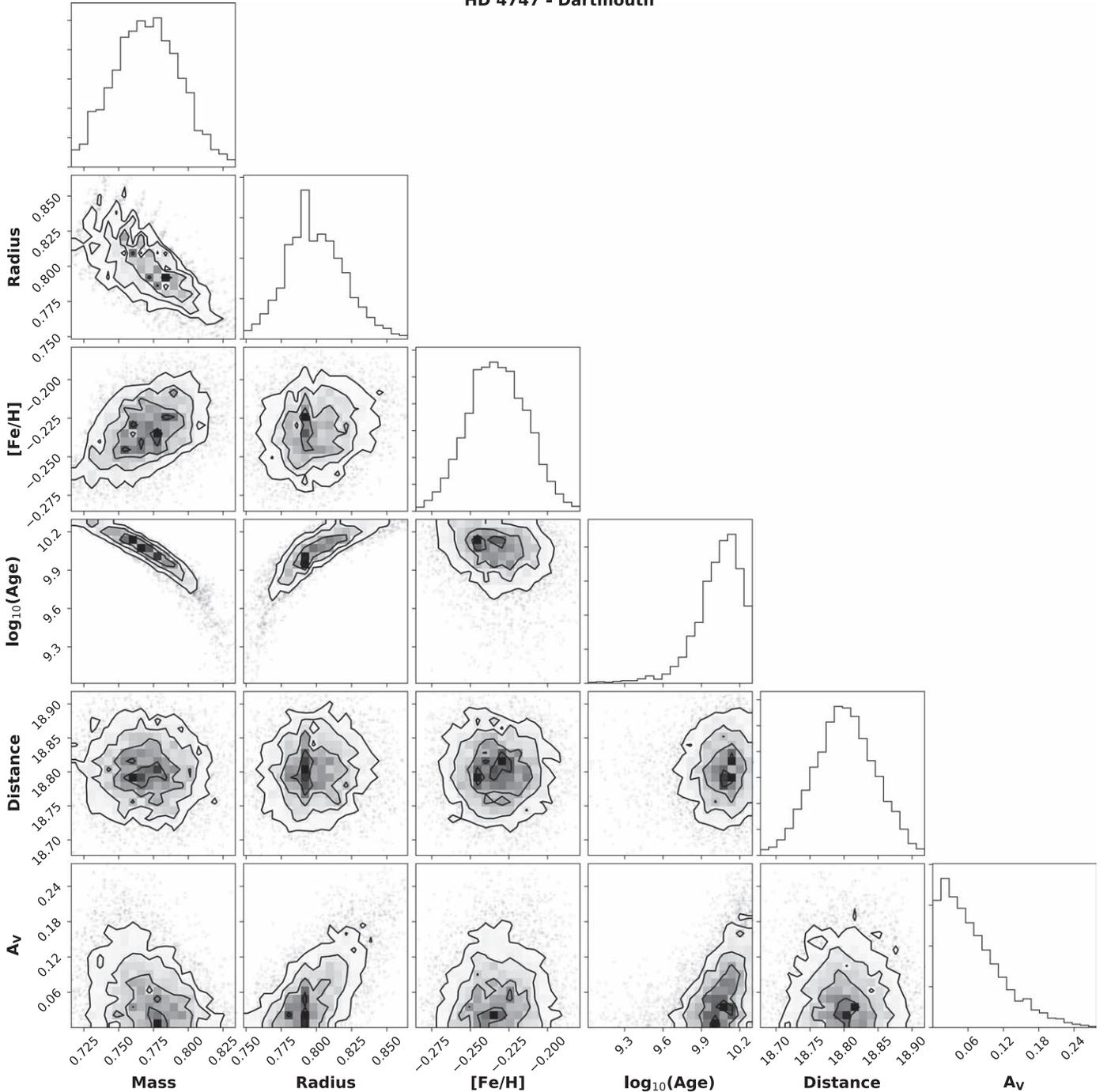
Figure 3. Corner plot for HD 4747 A from fitting the Dartmouth isochrones. The variables are (from left to right/top to bottom) mass, radius, [Fe/H], $\log_{10}$(age), and A_V of the star. The equivalent corner plot for HD 19467 A and corner plots for both stars from fitting the MIST isochrones are available in the figure set. See Section 4 for more information.

(The complete figure set (4 images) is available.)

The procedure uses forward modeling of 350 Å of the spectrum, first fitting for global parameters and deviations from a solar abundance pattern. It then fits for the abundances of 15 elements and repeats the entire procedure using this new abundance pattern. This method has been shown to recover surface gravities consistent with asteroseismology to within ±0.05 dex (Brewer et al. 2015). The effective temperatures obtained from the spectral fitting were consistent with those from the interferometric measurements (Table 2).

4.1. Yonsei-Yale Isochrones

With estimates for [Fe/H], [Si/H] (as a proxy for α-element enhancement), $T_{\rm eff}$, and bolometric luminosity we used the interpolation routines for the YY isochrones from Brewer et al. (2016) to derive masses, radii, surface gravities, and ages. The interpolation procedure does not allow us to utilize all of the constraints at our disposal, but the returned radii and surface gravities were consistent with our measured values.

Table 3
Summary of Isochronal Age Estimates (Gyr) for HD 4747 A and HD 19467 A

Isochrone	HD 4747 A	HD 19467 A
Dartmouth	$11.33^{+4.37}_{-4.25}$	10.66 ± 0.51
MIST	$11.49^{+4.25}_{-4.27}$	$10.66^{+0.50}_{-0.51}$
Yonsei-Yale	$9.39^{+2.90}_{-3.30}$	$8.85^{+0.92}_{-0.40}$
Adopted Age[a]	$10.74^{+6.75}_{-6.87}$	$10.06^{+1.16}_{-0.82}$

Note.
[a] Calculated as an average between the three age estimates. See Section 4.3.

Table 4
Properties of the Brown Dwarf Companions

Property	HD 4747 B[a]	HD 19467 B[b]
Spectral Type	$T1 \pm 2$	T5–T7
Separation (au)	11.3 ± 0.2	51.1 ± 1.0
[Fe/H]	-0.22 ± 0.04	-0.15 ± 0.02
$T_{\rm eff}$ (K)	1450 ± 50	1050 ± 40
Luminosity $(L_\odot)$[c]	$3.70 \pm 0.57 \times 10^{-5}$	$6.49 \pm 0.98 \times 10^{-6}$

Notes.
[a] Crepp et al. (2016, 2018).
[b] Crepp et al. (2014).
[c] This work (Section 5).

One constraint used that is not available for the other interpolation scheme is the Si/Fe ratio. Dotter (2016) showed that stars near their main-sequence turn-off will show an overall depletion of heavy elements in their atmospheres due to diffusion. The ratios of elements remain largely unchanged and so inclusion of this ratio may better capture the abundance of older main-sequence stars.

4.2. MIST and Dartmouth Isochrones

The isochrones package (Morton 2015) uses the MultiNest algorithm (Feroz & Hobson 2008; Feroz et al. 2009, 2013) to interpolate in either the MIST or Dartmouth isochrone grids. The routine allows for simultaneous fitting of many parameters, which we made use of to include additional constraints not possible with the YY isochrones. For both model grids, we fit the stars using our $T_{\rm eff}$, $\log g$, [Fe/H], radius, parallax from Gaia DR2 (Gaia Collaboration et al. 2018), and V magnitudes. The results of the fitting and correlations can be seen in the corner plots in Figure 3 and the figure set.

4.3. Isochrone Age Results

The results for both stars and all three isochrone grids is summarized in Table 3. Ages for HD 4747 A were consistent among the three different isochrone grids, though the uncertainties were large and the YY ages were lower by several gigayears. Low mass stars on the main sequence spend a large amount of time with only minimal changes in their temperature and brightness, making precise age determinations challenging. The YY age estimate for HD 19467 A was also lower than that for the MIST or Dartmouth estimates, which were again consistent with one another. In all three cases, HD 19467 A is fit to be on the subgiant branch and has much smaller age uncertainties due to the rapid evolution in this region.

The low age from the YY isochrones could be due to the inclusion of the Si/Fe ratio and its additional constraint on the initial metallicity. However, the MIST isochrones also place additional constraints on the initial metallicity by using surface abundances instead of initial abundances. Instead, the systematically lower ages from YY for both stars points to a difference in the stellar structure of the models at older evolutionary states, resulting in an age offset.

Unlike the Dartmouth and MIST isochrones, the YY isochrones do not allow us to include the surface gravity as a constraint. Since the surface gravities are consistent to within ± 0.05 dex of those from asteroseismology, we trust the Dartmouth and MIST age estimates over the YY age estimates; however, we still include the YY estimates in our analysis. We adopt ages that are averages of the Dartmouth, MIST, and YY estimates: $10.74^{+6.75}_{-6.87}$ Gyr for HD 4747 A and $10.06^{+1.16}_{-0.82}$ Gyr for HD 19467 A.

4.4. Discrepancies between Age Estimates

The gyrochronological age estimates for HD 4747 A ($3.3^{+2.3}_{-1.9}$ Gyr; Crepp et al. 2016) and HD 19467 A ($4.3^{+1.0}_{-1.2}$ Gyr; Crepp et al. 2014) are several gigayears younger than the isochronal age estimates. One possible explanation for this discrepancy is tidal interactions with a nearby companion "spinning up" the star (Brown 2014; Maxted et al. 2015). This seems unlikely, as the only known massive companions to both HD 4747 A and HD 19467 A are the benchmark brown dwarfs separated by $\rho = 11.3 \pm 0.2$ au and $\rho = 51.1 \pm 1.0$ au respectively. A more probable explanation is weakened magnetic braking, which occurs in solar-type stars with ages $\geqslant$4–5 Gyr (van Saders et al. 2016). This would result in gyrochronological age estimates of around 4 Gyr, despite the actual age of the star being older.

Isochronal models become less reliable as a star's properties deviate from those of the Sun (Bonaca et al. 2012; Tayar et al. 2017). However, both HD 4747 A and HD 19467 A are nearly Sun-like in mass, radius, luminosity, and metallicity, so we expect the isochronal models to be well-calibrated. In addition, gyrochronology is only precisely constrained for stars younger than the Sun (Mamajek & Hillenbrand 2008). As a result, we adopt the isochronal age estimates (Table 3) over the gyrochronological age estimates for both HD 4747 A and HD 19467 A.

To further investigate the discrepancy between isochronal and gyrochronological age estimates, the ages of HD 4747 A and HD 19467 A could be determined using asteroseismology (Ulrich 1986; Lebreton & Goupil 2014; Silva Aguirre et al. 2015). While neither star is on the TESS Asteroseismic Science Consortium (TASC) target list due to lower probabilities of detection of solar-like oscillations (about 5% for HD 4747 A and 20% for HD 19467 A; Campante et al. 2016), it is worth looking at because they are both relatively high on the Candidate Target List and should still be targeted with the two-minute cadence (Stassun et al. 2018). Other methods of determining age that are related to stellar activity or rotation, such as measuring lithium abundance or X-ray emission, would be correlated with the gyrochronological age and therefore not useful for resolving the discrepancy.
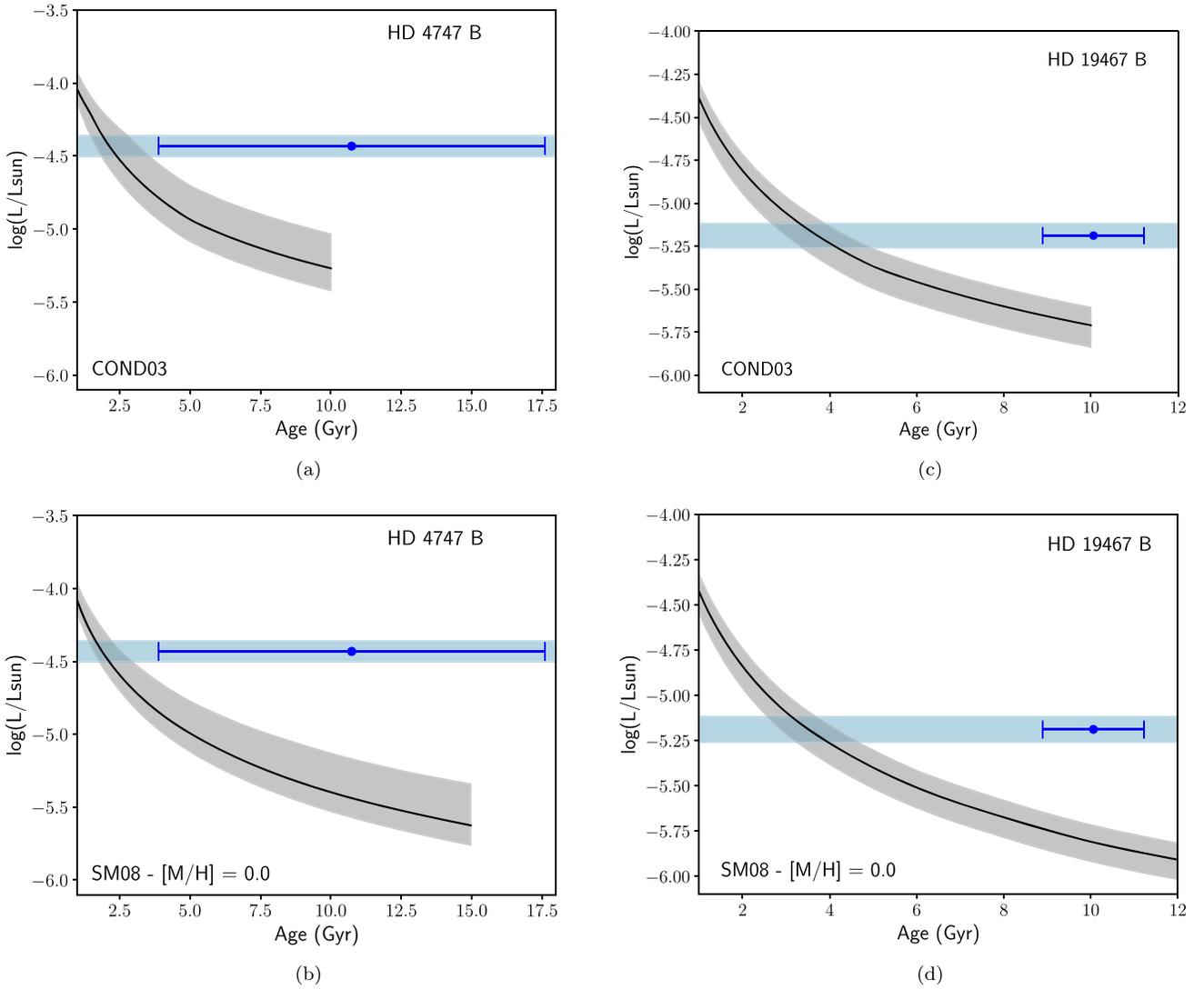
Figure 4. Luminosity vs. age comparison of the COND03 and SM08 substellar evolutionary models (black curves) to the observed data (blue dots) for HD 4747 B (a) and (b) and HD 19467 B (c) and (d). The light blue bars correspond to the uncertainty in the bolometric luminosities for the brown dwarfs. Although the models do not extend past 10 Gyr (COND03) and 15 Gyr (SM08), it is clear that they under-predict the bolometric luminosities of both objects because brown dwarfs do not sustain fusion and continuously cool. The models are too low by ∼0.75 dex for HD 4747 B and ∼0.5 dex for HD 19467 B. See Section 6.1.

5. Bolometric Luminosities of HD 4747 B and HD 19467 B

We calculate the bolometric luminosities of the brown dwarfs following the method outlined in Appendix A of Crepp et al. (2012) using the following equations:

$$M_{\rm bol} = M_{K_s} - 0.11 + BC_K \tag{2}$$

$$L = 10^{(M_{\rm bol,\odot} - M_{\rm bol})/2.5} L_\odot, \tag{3}$$

where the bolometric magnitude of the Sun $M_{\rm bol,\odot} = 4.74$.

HD 4747 B has an absolute magnitude $M_{K_s} = 13.00 \pm 0.14$ (Crepp et al. 2016). Combined with the 0.11 mag correction to convert to M_K (Rudy et al. 1996) and an estimated bolometric correction $BC_K = 2.93 \pm 0.09$ (Golimowski et al. 2004) using the updated spectral type and temperature from Crepp et al. (2018), we obtain a bolometric magnitude $M_{\rm bol} = 15.82 \pm 0.17$. This gives us a bolometric luminosity $L = (3.70 \pm 0.57) \times 10^{-5} L_\odot$.

HD 19467 B has an absolute magnitude $M_{K_s} = 15.52 \pm 0.10$ (Crepp et al. 2014). Combined with the 0.11 mag correction to convert to M_K (Rudy et al. 1996) and an estimated bolometric

correction $BC_K = 2.30 \pm 0.13$ (Golimowski et al. 2004), we obtain a bolometric magnitude $M_{\rm bol} = 17.71 \pm 0.16$. This gives us a bolometric luminosity $L = (6.49 \pm 0.98) \times 10^{-6} L_\odot$. See Table 4 for a complete list of brown dwarf properties.

6. Comparison to SSEMs

Assuming the brown dwarf companions HD 4747 B and HD 19467 B have the same ages as their respective host stars, we can directly test the accuracy of several SSEM. For this paper, we looked at SSEMs from Baraffe et al. (2003; COND03), Baraffe et al. (2015; BHAC15), and Saumon & Marley (2008; SM08) and compared them to calculated properties of HD 4747 B and HD 19467 B both graphically and numerically.

6.1. Visual Comparisons

We directly compare the calculated bolometric luminosities (Section 5) for the brown dwarfs to the theoretical predictions from each SSEM given their dynamical masses and isochronal
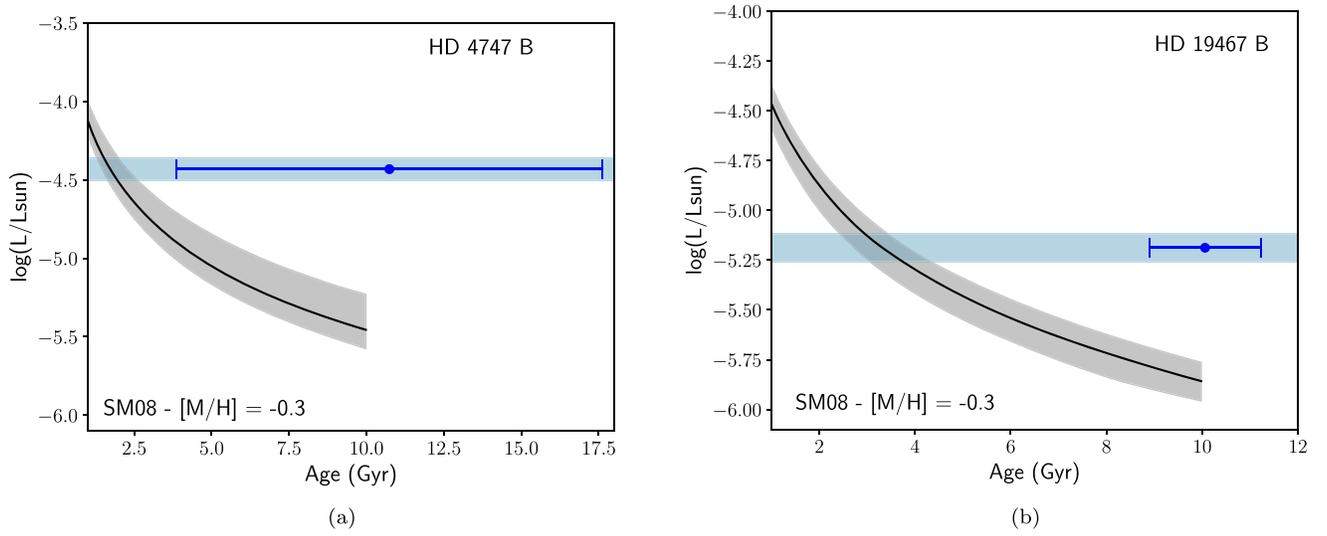
Figure 5. Luminosity vs. age comparison of the lower metallicity SM08 substellar evolutionary model (black curves) to the observed data (blue dots) for HD 4747 B (a) and HD 19467 B (b). The light blue bars correspond to the uncertainty in the bolometric luminosities for the brown dwarfs. For both HD 4747 B and HD 19467 B, the lower metallicity model increases the discrepancy to ∼1 dex and ∼0.7 dex respectively. See Section 6.1.1.
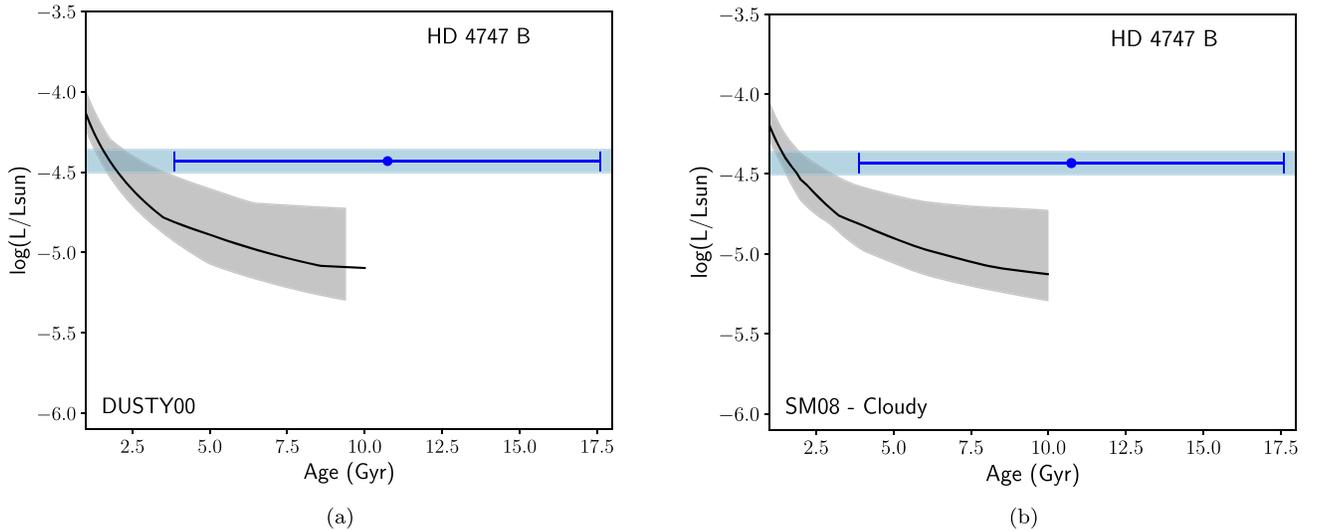
Figure 6. Luminosity vs. age comparison of the DUSTY00 and SM08-C substellar evolutionary models (black curves) to the observed data (blue dots) for HD 4747 B. The light blue horizontal bars correspond to the uncertainty in the bolometric luminosity for the brown dwarf. The cloudy models predict the luminosity of HD 4747 B better than the cloudless models, reducing the discrepancy to ∼0.6 dex. See Section 6.1.2.

Table 5
Photometric Masses of HD 4747 B and HD 19467 B

Object	Dynamical[a]	COND03	SM08	DUSTY00	SM08-C
HD 4747 B	$65.3^{+4.4}_{-3.3}$	$72.7^{+3.4}_{-13.6}$	$74.3^{+1.2}_{-11.5}$	$69.7^{+1.6}_{-13.6}$	$71.7^{+1.2}_{-9.3}$
HD 19467 B	$51.9^{+3.6}_{-4.3}$	$67.3^{+0.9}_{-1.2}$	$68.6^{+1.2}_{-1.6}$	⋯	⋯

Notes. Masses reported in units of M_{Jup}.
[a] Crepp et al. (2018, 2014).

age estimates. Each SSEM is linearly interpolated across ages and masses using the SciPy (Jones et al. 2001) algorithm `LinearNDInterpolator` to give a grid of bolometric luminosity predictions, with age and mass spanning ranges determined by the extent of each model.[11] We then plot the

---

[11] Ages generally range from 0.0010 to 10 Gyr and masses generally range from 0.001 to 0.072 $M_{\odot}$.

SSEM linear interpolations with the data points for each brown dwarf to see if they are consistent (Figure 4).

We find that the COND03 and SM08 SSEMs under-predict the bolometric luminosities of both brown dwarf companions, which is consistent with previous tests of SSEMs using benchmark brown dwarfs (Dupuy et al. 2009b, 2014; Crepp et al. 2012, 2018). The model predictions are too low by ∼0.75 dex for HD 4747 B at the best-fit age and mass and

~0.5 dex for HD 19467 B. If the masses of both objects are slightly higher, which has been suggested for HD 4747 B (Peretti et al. 2018), the measured bolometric luminosity would be more consistent with the models. For HD 4747 B, increasing the mass places the object around the hydrogen burning limit, increasing the range in the predicted luminosity. We do not make any conclusions regarding the BHAC15 models at this time as they currently do not extend to ages older than ~2 Gyr for masses lower than 0.080 $M_\odot$.

6.1.1. Effects of Metallicity on Luminosity Predictions

There are few SSEMs available that explore the effect of metallicity on brown dwarf evolution. Of the models tested, only Saumon & Marley (2008) provide grids for metallicities other than solar. To effectively explore how metallicity changes the luminosity predictions of brown dwarfs, SSEMs that span a wider range of metallicities are needed, such as the upcoming Sonora models (Marley et al. 2017).

Since both HD 4747 B and HD 19467 B have metallicities slightly less than solar, we compare them to the grid assuming $[M/H] = -0.3$ (Figure 5). In both cases, this comparison does not improve the discrepancy between the calculated and predicted bolometric luminosities. The lower metallicity model under-predicts the bolometric luminosity for HD 4747 B by ~1 dex and ~0.7 dex for HD 19467 B.

6.1.2. Effects of Clouds on Luminosity Predictions for HD 4747 B

HD 4747 B is an early T-dwarf (spectral type T1 ± 2) near the L/T transition, where its atmosphere is cool enough to begin forming clouds (Crepp et al. 2016, 2018). To account for this, we also compare HD 4747 B to SSEMs that include cloud formation by Chabrier et al. (2000) and Baraffe et al. (2002; DUSTY00) and Saumon & Marley (2008; SM08-C; Figure 6). The cloudy models are a closer fit to the data for HD 4747 B than the cloudless models, reducing the discrepancy in the bolometric luminosity to ~0.6 dex.

6.2. Photometric Mass Estimates

Using a Markov Chain Monte Carlo (MCMC) simulation, we calculate the photometric mass of HD 4747 B and HD 19467 B according to each SSEM given their isochronal ages and bolometric luminosities. We perform the MCMC simulation using the Python package emcee (Foreman-Mackey et al. 2013), which implements an affine-invariant ensemble sampler to explore our three-dimensional (age, mass, and luminosity) parameter space with Gaussian priors on age and luminosity and a Gaussian likelihood function for mass. The results of the MCMC are shown in Table 5.

As expected based on our plots from Section 6.1, the predicted photometric masses for both HD 4747 B and HD 19467 B are higher (~12% and ~30% respectively) than the dynamical mass measurements when considering the cloudless models. For HD 19467 B, the models are discrepant by about 4σ. Due to the larger lower bound errors from the models for HD 4747 B, the cloudless models are consistent with the dynamical mass. When comparing to the cloudy models, the predicted mass for HD 4747 B is reduced to ~8% higher than the dynamical mass, which is still consistent within 1σ.

7. Summary and Conclusions

For brown dwarfs found as companions to stars, certain properties such as metallicity and age can be determined independent from the brown dwarf's mass and luminosity by studying the host star instead of the brown dwarf. As a result, such objects are ideal to use as benchmarks for SSEMs. While not many are known, benchmark brown dwarfs tend to be over-luminous compared to SSEMs.

Using new age estimates for HD 4747 B and HD 19467 B, determined by studying the host stars with interferometry, we have shown that current SSEMs under-predict the bolometric luminosities and over-predict the masses of these brown dwarfs. Our discrepancy between measured and predicted bolometric luminosities is high compared to previous results for HD 130948 BC and HR 7672 B (Dupuy et al. 2009b; Crepp et al. 2012), but the discrepancy between measured and predicted masses is consistent with results for Gl 417 BC (Dupuy et al. 2014). Since both HD 4747 B and HD 19467 B orbit far from their host stars, we do not expect this additional luminosity to result from heating due to the star.

Although including clouds in the SSEMs puts the predicted mass and luminosity of HD 4747 B in better agreement with the measured data, the brown dwarf still appears over-luminous. A possible explanation for the remaining discrepancy is missing physics in the models. The effect of metallicity on brown dwarf atmospheres is one area of improvement that has yet to be fully explored in SSEMs. The presence of additional metals could affect the amount of cloud formation and which condensates are formed, both of which would affect the opacity of the atmosphere and therefore the observed luminosity of the brown dwarf (Marley & Robinson 2015). Future SSEMs such as the Sonora models (Marley et al. 2017) plan to cover a wider range of metallicities.

To improve the comparisons of HD 4747 B and HD 19467 B to SSEMs, more study should be done to constrain the masses and the ages of the brown dwarfs. Mass estimates will be improved with more radial velocity and direct imaging data combined with the latest parallaxes from *Gaia* DR2 (Brandt et al. 2018). Current age estimates are highly disparate and method-dependent. Although neither HD 4747 A nor HD 19467 A are on the TASC target list, both stars should be targeted with the TESS two-minute cadence and could be studied with asteroseismology to help resolve the age discrepancy.

ORCID iDs

Charlotte M. Wood ⓘ https://orcid.org/0000-0003-4773-4602
Tabetha Boyajian ⓘ https://orcid.org/0000-0001-9879-9313
Kaspar von Braun ⓘ https://orcid.org/0000-0002-5823-4630
John M. Brewer ⓘ https://orcid.org/0000-0002-9873-1471
Justin R. Crepp ⓘ https://orcid.org/0000-0003-0800-0593
Gail Schaefer ⓘ https://orcid.org/0000-0001-5415-9189
Arthur Adams ⓘ https://orcid.org/0000-0002-7139-3695
Timothy R. White ⓘ https://orcid.org/0000-0002-6980-3392

References

Aumer, M., & Binney, J. J. 2009, MNRAS, 397, 1286
Baraffe, I., Chabrier, G., Allard, F., & Hauschildt, P. H. 2002, A&A, 382, 563
Baraffe, I., Chabrier, G., Barman, T. S., Allard, F., & Hauschildt, P. H. 2003, A&A, 402, 701
Baraffe, I., Homeier, D., Allard, F., & Chabrier, G. 2015, A&A, 577, A42
Bohlin, R. C., Gordon, K. D., & Tremblay, P.-E. 2014, PASP, 126, 711
Bonaca, A., Tanner, J. D., Basu, S., et al. 2012, ApJL, 755, L12
Boyajian, T., von Braun, K., Feiden, G. A., et al. 2015, MNRAS, 447, 846
Boyajian, T. S., McAlister, H. A., van Belle, G., et al. 2012a, ApJ, 746, 101
Boyajian, T. S., van Belle, G., & von Braun, K. 2014, AJ, 147, 47
Boyajian, T. S., von Braun, K., van Belle, G., et al. 2012b, ApJ, 757, 112
Boyajian, T. S., von Braun, K., van Belle, G., et al. 2013, ApJ, 771, 40
Brandt, T. D., Dupuy, T., & Bowler, B. P. 2018, arXiv:1811.07285
Brewer, J. M., Fischer, D. A., Basu, S., Valenti, J. A., & Piskunov, N. 2015, ApJ, 805, 126
Brewer, J. M., Fischer, D. A., Valenti, J. A., & Piskunov, N. 2016, ApJS, 225, 32
Brown, D. J. A. 2014, MNRAS, 442, 1844
Campante, T. L., Schofield, M., Kuszlewicz, J. S., et al. 2016, ApJ, 830, 138
Chabrier, G., Baraffe, I., Allard, F., & Hauschildt, P. 2000, ApJ, 542, 464
Chelli, A., Duvert, G., Bourgès, L., et al. 2016, A&A, 589, A112
Choi, J., Dotter, A., Conroy, C., et al. 2016, ApJ, 823, 102
Claret, A., & Bloemen, S. 2011, A&A, 529, A75
Corben, P. M. 1971, MNSSA, 30, 37
Corben, P. M., Carter, B. S., Banfield, R. M., & Harvey, G. M. 1972, MNSSA, 31, 7
Crepp, J. R., Gonzales, E. J., Bechter, E. B., et al. 2016, ApJ, 831, 136
Crepp, J. R., & Johnson, J. A. 2011, ApJ, 733, 126
Crepp, J. R., Johnson, J. A., Fischer, D. A., et al. 2012, ApJ, 751, 97
Crepp, J. R., Johnson, J. A., Howard, A. W., et al. 2014, ApJ, 781, 29
Crepp, J. R., Principe, D. A., Wolff, S., et al. 2018, ApJ, 853, 192
Cutri, R. M., Skrutskie, M. F., van Dyk, S., et al. 2003, yCat, 2246
Dotter, A. 2016, ApJS, 222, 8
Dotter, A., Chaboyer, B., Jevremović, D., et al. 2007, AJ, 134, 376
Dotter, A., Chaboyer, B., Jevremović, D., et al. 2008, ApJS, 178, 89
Dupuy, T. J., & Liu, M. C. 2017, ApJS, 231, 15
Dupuy, T. J., Liu, M. C., & Ireland, M. J. 2009a, ApJ, 699, 168
Dupuy, T. J., Liu, M. C., & Ireland, M. J. 2009b, ApJ, 692, 729
Dupuy, T. J., Liu, M. C., & Ireland, M. J. 2014, ApJ, 790, 133
Duvert, G. 2016, yCat, 2345
Eggen, O. J. 1983, AJ, 88, 813
Feroz, F., & Hobson, M. P. 2008, MNRAS, 384, 449
Feroz, F., Hobson, M. P., & Bridges, M. 2009, MNRAS, 398, 1601
Feroz, F., Hobson, M. P., Cameron, E., & Pettitt, A. N. 2013, arXiv:1306.2144
Foreman-Mackey, D. 2016, JOSS, 1, 24
Foreman-Mackey, D., Hogg, D. W., Lang, D., & Goodman, J. 2013, PASP, 125, 306
Gaia Collaboration, Brown, A. G. A., Vallenari, A., et al. 2018, A&A, 616, A1
Golimowski, D. A., Leggett, S. K., Marley, M. S., et al. 2004, AJ, 127, 3516
Hauck, B., & Mermilliod, M. 1998, A&AS, 129, 431
Ireland, M. J., Mérand, A., ten Brummelaar, T. A., et al. 2008, Proc. SPIE, 7013, 701324
Irwin, J. B. 1961, ApJS, 6, 253
Jones, E., Oliphant, T., Peterson, P., et al. 2001, SciPy: Open Source Scientific Tools for Python, http://www.scipy.org/
Koen, C., Kilkenny, D., van Wyk, F., & Marang, F. 2010, MNRAS, 403, 1949
Kornilov, V., Mironov, A., & Zakharov, A. 1996, BaltA, 5, 379
Lebreton, Y., & Goupil, M. J. 2014, A&A, 569, A21
Liu, M. C., Dupuy, T. J., & Ireland, M. J. 2008, ApJ, 689, 436
Maestro, V., Che, X., Huber, D., et al. 2013, MNRAS, 434, 1321
Mamajek, E. E., & Hillenbrand, L. A. 2008, ApJ, 687, 1264
Mann, A. W., Gaidos, E., & Ansdell, M. 2013, ApJ, 779, 188
Mann, A. W., & von Braun, K. 2015, PASP, 127, 102
Marley, M. S., & Robinson, T. D. 2015, ARA&A, 53, 279
Marley, M. S., Saumon, D., Fortney, J. J., et al. 2017, AAS Meeting, 230, 315.07
Maxted, P. F. L., Serenelli, A. M., & Southworth, J. 2015, A&A, 577, A90
Mermilliod, J.-C. 1986, BICDS, 31, 185
Mermilliod, J. C., & Nitschelm, C. 1989, A&AS, 81, 401
Morton, T. D. 2015, Isochrones: Stellar Model Grid Package, Astrophysics Source Code Library, ascl:1503.010
Olsen, E. H. 1983, A&AS, 54, 55
Olsen, E. H. 1993, A&AS, 102, 89
Olsen, E. H. 1994, A&AS, 106, 257
Paxton, B., Bildsten, L., Dotter, A., et al. 2011, ApJS, 192, 3
Paxton, B., Cantiello, M., Arras, P., et al. 2013, ApJS, 208, 4
Paxton, B., Marchant, P., Schwab, J., et al. 2015, ApJS, 220, 15
Peretti, S., Ségransan, D., Lavie, B., et al. 2018, arXiv:1805.05645
Pickles, A. J. 1998, PASP, 110, 863
Rudy, R. J., Rossano, G. S., & Puetter, R. C. 1996, ApJL, 458, L41
Rufener, F. 1988, A&AS, 78, 469
Saumon, D., & Marley, M. S. 2008, ApJ, 689, 1327
Silva Aguirre, V., Davies, G. R., Basu, S., et al. 2015, MNRAS, 452, 2127
Spada, F., Demarque, P., Kim, Y.-C., & Sills, A. 2013, ApJ, 776, 87
Stassun, K. G., Oelkers, R. J., Pepper, J., et al. 2018, AJ, 156, 102
Stoy, R. H. 1963, MNSSA, 22, 157
Tayar, J., Somers, G., Pinsonneault, M. H., et al. 2017, ApJ, 840, 17
ten Brummelaar, T. A., McAlister, H. A., Ridgway, S. T., et al. 2005, ApJ, 628, 453
Ulrich, R. K. 1986, ApJL, 306, L37
van Belle, G. T., & van Belle, G. 2005, PASP, 117, 1263
van Saders, J. L., Ceillier, T., Metcalfe, T. S., et al. 2016, Natur, 529, 181
Vogt, S. S., Allen, S. L., Bigelow, B. C., et al. 1994, Proc. SPIE, 2198, 362
von Braun, K., Boyajian, T. S., van Belle, G. T., et al. 2014, MNRAS, 438, 2413
White, T. R., Huber, D., Maestro, V., et al. 2013, MNRAS, 433, 1262
Wild, P. A. T. 1969, MNSSA, 28, 123